Int. J. Electrochem. Sci., 14 **(2019)** 10139 – 10152, doi: 10.20964/2019.11.07

International Journal of
ELECTROCHEMICAL
SCIENCE
www.electrochemsci.org

Electrochemical mechanism of 317L stainless steel under biofilms with coexistence of iron-oxidizing bacteria and sulfate-reducing bacteria

Haiya Zhang[1,2], *Yimei Tian*[1,*], *Mengxin Kang*[1], *Shichao Jia*[1]

[1] School of Environmental Science and Engineering, Tianjin University, Tianjin, 300350, China
[2] School of Environment, Tsinghua University, Beijing 100084, China
[*]E-mail: ymtian_2000@126.com

Received: 14 April 2019 / *Accepted:* 22 August 2019 / *Published:* 7 October 2019

The corrosion behavior of 317L stainless steel (SS) in the presence of biofilms with coexistence of iron-oxidizing bacteria (IOB) and sulfate-reducing bacteria (SRB) was investigated by polarization curves and electrochemical impendence spectra. Results showed that the corrosion mechanisms varied with the bacterial evolution process. the lower dissolved oxygen (DO) concentration caused by the IOB multiplication in reclaimed water induced the ennoblement of E_{corr} and the increase of electron transfer resistance due to the fact that DO using as the only depolarization agent. Meanwhile, the deposition of an outer IOB biofilm, iron hydroxide layer and an inner chromium oxide layer on the 317L SS protected the metal surface and retarded the corrosion process. However, as the SRB proliferation the cathode depolarization process was promoted by SRB metabolic activity after 5 days and the preformed two-layer films were converted into one layer induced by the sulfidation effect, enhancing the electron transfer process correspondingly. Furthermore, the uneven metabolisms distribution, gradients of sulfate ions and DO concentration and heterogeneous biofilm structure induced larger localized corrosion of 317L SS by biofilm in reclaimed water.

Keywords: electrochemical corrosion mechanisms; 317L stainless steel; biofilm; IOB; SRB; reclaimed water

1. INTRODUCTION

Corrosion is one of the most common phenomena when utilizing metallic materials, which was often induced by chemical or electrochemical reactions between the electrolyte and metal surface. Microbial activity was reported as one of the most important factors affecting the electrochemical corrosion process, which also presented a strong tendency to attach on the metal surface and form biofilms [1, 2]. Biofilm formation not only change the physical/chemical conditions on the metal surface

but also alter the anodic/cathodic half-reactions on the metal/solution interface, and cause microbiologically influenced corrosion (MIC) [3, 4].

Many types of microorganisms could cause metal corrosion. Sulfate-reducing bacteria (SRB) have been reported to be one of the most common bacteria, which contributed to half of the MIC in industry [5-7]. The mechanisms that explain the SRB effect on corrosion included cathodic depolarization, iron sulfide accumulation, and local acidification [8-10]. Moreover, SRB cells also tend to form biofilms by producing extracellular polymeric substances, enhancing the hydrogen sulfides production and intrinsic heterogeneity, and modifying the physicochemical microenvironments [10]. Most of these research have focused on single isolated SRB species [11]. However, microbiologically influenced corrosion is a complicated process that might be related to other bacteria. Therefore, the other symbiotic bacteria may also affect the activity and characteristics of SRB, and change the corrosion mechanism furthermore.

Recently, the corrosion process induced by the coexistence of different bacteria had attracted voluminous attention [12, 13]. Wadood revealed that an antagonistic interaction was found between *Pseudomonas aeruginosa* and *Bacillus subtilis* in mixed-species biofilms, which made the corrosion rate lower than that in a single-species environments [14]. Wu reported that the corrosion rate was lower in media containing *Desulfovibrio sp.* and *Pseudoalteromonas sp.* than that in media containing only *Desulfovibrio sp*. Similarly, the cast-iron corrosion in the co-presence of *P. aeruginosa* and *D. vulgaris* (SRB) was diminished compared to that in the presence of the SRB alone [15]. These results demonstrated the corrosion inhibition effect of *Pseudoalteromonas sp.* when coexistence with *Desulfovibrio sp* [16]. However, some studies also found that the corrosion rate was accelerated by *P. aeruginosa* and *Klebsiella pneumonia* when the dissolved oxygen concentration was lower than<1.5 mg/L. Thus, this problem is complex when considering the concurrence of different bacteria because the interaction between different microbial populations varied significantly (aerobic and anaerobic bacteria) [8, 14, 17]. Consequently, further research is needed to understand the underlying mechanisms of biofilm-induced corrosion under the combined conditions of different bacteria.

Iron-oxidizing bacteria (IOB) have been reported as another main group of corrosive bacteria, which can coexist with SRB in naturally occurring biofilms. The stainless steel (SS) was widely used in pipelines and structural materials in the reclaimed water environment due to its high corrosion resistance and excellent electrical and thermal conductivity [18].The good corrosion resistance of SS might be attributable to the formation of a thin passive film due to the presence of chromium (Cr), nickel (Ni), manganese (Mn), or other elements in its metallurgical formulation [14]. Many studies focused the effect of aerobic bacteria on different alloys [19]. Starosvetsky reported that the IOB induced crevice corrosion for stainless steel [12]. Additionally, the corrosion rate of 2507 duplex stainless steel in the presence of *B. vietnamensis* was reported increased significantly [19]. Moradi reported the activity of IOB on 316 SS could change the chemical composition of intermetallics and corrosion products [20]. All these studies demonstrated the complexity of MIC caused by aerobic bacteria on different metals. However, MIC behavior of 317L SS has received less attention and there is still no clear relationship between the IOB and SRB activity on the electrochemical corrosion behavior, especially considering the changes on the preformed passive layer [21].

The present study aimed at investigating the electrochemical corrosion mechanisms of 317L SS in the presence of biofilms with coexistence of IOB and SRB by using the electrochemical and surface analytical techniques. Polarization curves and electrochemical impendence spectra (EIS) were collected to evaluate the electrochemical corrosion mechanisms The scanning electron microscope (SEM) and 3D stereoscopic microscope were used to analyze the surface morphology and the localized corrosion phenomena. Additionally, Energy Dispersive Spectrometer (EDS) was used to evaluate the elemental composition of the corrosion products.

2. MATERIALS AND METHODS

2.1 Stainless steel coupons and working electrodes

All stainless steel coupons in this work were manufactured according to HG/T 3523-2008. The coupons were with a chemical composition (wt, %) of 19.0 C, 3.4 P, 1.63 Mn, 4.4 Si, 0.58 S, 12.78 Ni, 18.62 Cr, and 3.14 Mo, with Fe making up the balance. The dimensions of the rectangle coupons were 72.4 × 11.5 × 2.0 mm. Exceptionally, the coupons were cut into a cylinder with cross-section of 0.5 cm^2 to make as the working electrodes. Subsequently, the cylinders were grounded with the waterproof abrasive papers sequentially (200#, 400#, 600#, 800#, 1000#, 1200# and 1500#), welded with a metal wire, and sealed with epoxy resin. Afterwards, these electrodes were degreased in acetone, dehydrated in anhydrous ethanol, vacuum-dried and disinfected with ultraviolet (UV) radiation for 30 min before used.

2.2 Bacterial incubation and cells counting

IOB and SRB species were isolated from effluent water in running annular reactors (ARs). Additionally, reclaimed water treated with high temperature sterilization was used as the sterile control water (pH: 8.86±0.5). After sterilization, the total bacterial count was <1 CFU/mL. The culture medium for microorganisms was R_2A, which was autoclaved at 121 °C for 20 min before being used. The volume ratio of reclaimed water to culture medium was 1:10. Sterile water without microorganisms was also added into the culture medium in the same proportion as the control. Moreover, in order to maintain a sterile environment, the ultraviolet light was always irradiated throughout the control experiments.

The prepared 317L SS coupons and working electrodes were immersed into lightproof, 250 ml ground-glass stoppered bottles containing reclaimed water or sterile water. For the duration of the experiment, the bottles were placed in a biochemical incubator at 30°C. The coupons were extracted from the bottles to obtain bacterial data at predetermined cultivation times (1, 5, 10, 20, and 40 days). Three parallel coupons were prepared under each conditions to ensure the reproducibility of results. The coupons were washed gently with aseptic water and immersed in an ultrasonic cleaning system with 0.01 M phosphate buffer solution (PBS) for 20 min to obtain the biofilm bacteria solution. Finally, the counts of IOB and SRB were determined by the maximum probable number (MPN) approach according to the Chinese National Standards (GB/T 14643.5-2009; GB/T 14643.5-2009). All biofilm results were

normalized to the surface area (1 cm^2). Additionally, water quality parameters such as DO and sulfate ion (SO_4^{2-}) content were measured according to standard methods (GB5749-2006).

2.3 Biofilm analysis

Immediately after the coupons were removed from the incubation bottles, they were washed twice with deionized water, then immersed in 2.5% glutaraldehyde fixation fluid for 2 h at 4 °C in a refrigerator for biofilm fixation. The coupons were then sequentially immersed into ethanol with different concentrations for dehydration. The biofilm morphology and elemental composition were examined by an S4800 field emission SEM (Hitachi Company, Tokyo, Japan) equipped with a Genesis XM2 EDS (EDS Company, Dallas, USA). The scanning ranges of the electron microscope were from 1 μm to 10 μm. Prior to SEM observation, the coupons were coated with a thin gold film (0.5 μm) to improve the electrical conductivity. Additionally, the localized corrosion profile after the removal of corrosion products was measured by a 3D stereoscopic microscope (Hirox KH-7700, Hirox CO., Ltd, Tokyo, Japan).

2.4 Electrochemical measurements

To understand the electrochemical corrosion mechanisms of 317L SS, potentiodynamic polarization and EIS were performed with a CS350 electrochemical working station (KeSiTe company, WuHan, China). Reclaimed water or sterile water with culture medium was used as electrolyte, a high-purity platinum sheet (99.99%) with a total area of 1 cm^2 was used as the counter electrode, and Ag/(AgCl) (saturated KCl) was used as the reference electrode. The potentiodynamic polarization curves were acquired with a potential range of -0.1 V to 0.1 V versus open circuit potential at a scan rate of 0.5 mV/s. The EIS measurements were performed with an applied sinusoidal voltage of 10 mV and a frequency ranging from 0.01 to 100000 Hz. The acquired data was fitted and simulated by Zsimpwin (Version 3.10) based on the appropriate equivalent circuit models.

3. RESULTS AND DISCUSSION

3.1 Water quality and biofilm bacteria analysis

The variation of IOB and SRB bacterial counts, the sulfate anions and dissolved oxygen (DO) concentrations in reclaimed water and sterile water over time can be seen in Fig. 1. The DO concentration in sterile water declined slightly from 7.88 mg/L to 6.02 mg/L within 40 days, indicating the oxygen consumption caused by the metal corrosion process. Similarly, the DO concentration in reclaimed water also presented a declining trend throughout the experiments, while, the values were much lower than those in the bulk control, which might be caused by the rapid bacterial growth. IOB is aerobic bacteria, which can obtain energy through the iron oxidation process. Therefore, its growth strongly depends on DO concentration and the metal matrix [12]. Fig. 1 also showed that the IOB counts increased gradually

to the maximum value of 10672 CFU/mL·cm^2 after 10 days of incubation, while, which decreased gradually to 6530 CFU/mL·cm^2 at 40 days due to the decreased DO concentration and accumulated corrosion products.

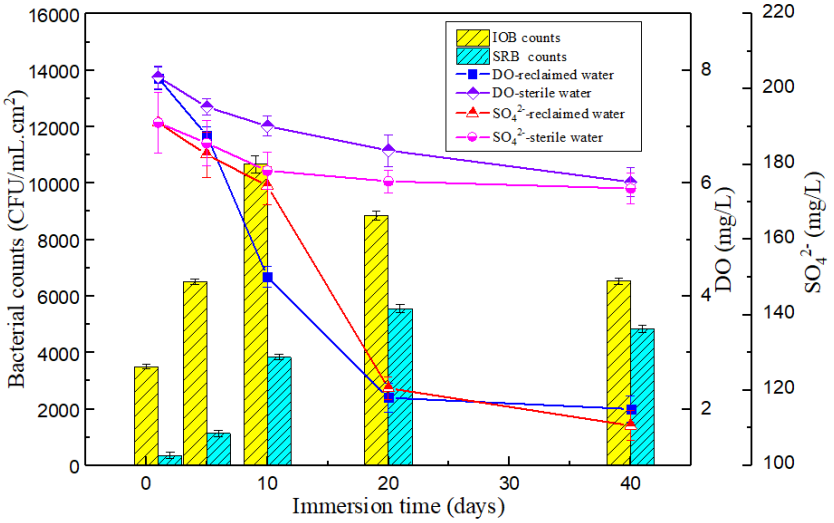

Figure 1. Variation of IOB and SRB counts, sulfate anions and DO concentration over time

The concentration of sulfate in sterile water presented slightly downward trend due to the adsorption of corrosion products. And, no significant difference of sulfate anions concentration between the reclaimed water and sterile water in the first 10 days were found, showing no significant microbial metabolic activity involving sulfur occurred at this time. Thus, SRB counts did't experience a significant growth initially. This is because DO could't be scavenged completely by the activity of IOB in aerobic environment, thus inhibiting the growth of SRB. This results also illustrated the toxicity of oxygen to SRB [22].

However, the DO concentration decreased rapidly after 20 days and the values of sulfate ions concentration were much lower in reclaimed water than those in sterile water, demonstrating the rapid proliferation of SRB in the former experiments. All the above results illustrated the fact that bacteria colonization in reclaimed water is a dynamic and continuous process, in which IOB and SRB growth, proliferation and decline. And this bacterial evolution process might affect the 317L SS corrosion greatly.

3.2 Morphology of corrosion products and biofilm

The micro-morphologies of corrosion-product and biofilms on the 317L SS surface after 40 days of incubation were inspected (Fig. 2). The chemical compositions of these films are shown in Table 1. Clear differences in corrosion morphology were found between these two systems. The smooth metal base could be seen in sterile water with the observation range of 10 μm, while when viewed at a smaller scale at 1 μm, blocky corrosion products were visible. EDS results showed that high proportion of element Fe and O were found in the outer corrosion product layer in sterile water at 5 days and 40 days probably due to the formation of iron oxides or iron hydroxides. Additionally, the element chromium

and nickel were evident in the inner corrosion layer, indicating the formation of a passive layer containing chromium oxides and nickel oxides.

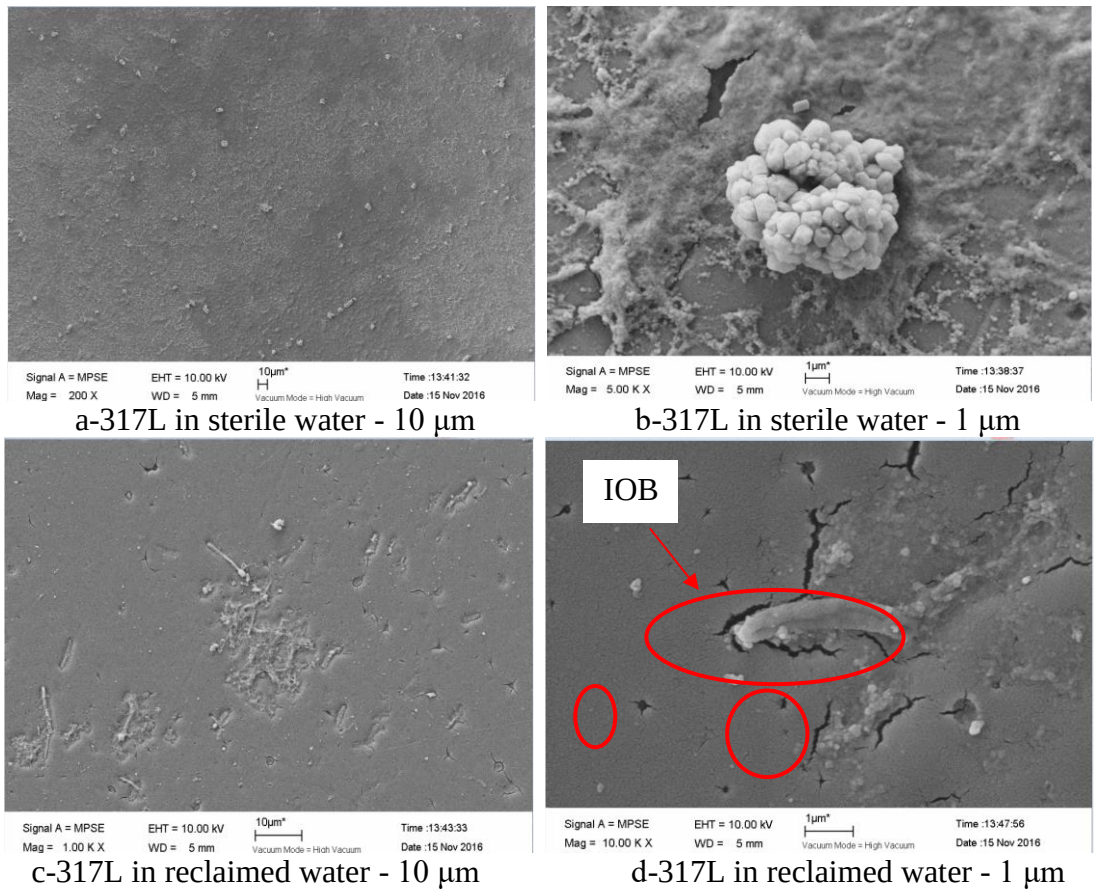

Figure 2. SEM images of corrosion products on the 317L SS surface in sterile water at 40 days (a, b); and biofilm on the 317L SS surface in reclaimed water at 40 days (c, d)

Table 1. Elemental composition of the 317L surface in sterile water (S) and reclaimed water (R) at typical time

Element (%)	C	O	Cl	Fe	Ni	Cr	S	Mo
S-1 day	11.32	12.56	0.2	40.01	15.62	13.43	0.02	6.84
S-5 days-outer layer	15.35	22.88	0.26	52.7	2.15	1.31	5.35	0
S-5 days-inner layer	6.23	9.13	0.11	0.21	36.64	40.78	1.28	5.62
S-40 days-outer layer	10.58	10.35	0.18	32.3	18.56	22.41	5.62	0
S-40 days-inner layer	5.28	9.56	0.08	3.68	34.68	38.78	1.56	6.38
R-1 day	20.37	23.33	0.2	36.5	9.2	10.35	0.05	0
R-5 days-outer layer	31.9	25.02	0.32	40.97	0.62	0.97	0.2	0
R-5 days-inner layer	2.15	13.65	0.19	2.19	34.32	40.14	0.78	6.58
R-40 days	17.71	3.98	0.16	28.55	20.25	16.07	13.28	0

In reclaimed water experiments at 5 days, the percentages of element Fe, C and O in the outer layer of the 317L SS were 40.97%, 31.90% and 25.02%, accounting for 97.89% of the total elements in

outer layer. These results (in conjunction with the EIS results) likely indicated that the IOB cells, bacterial metabolic products and iron corrosion products might mixed together as a whole and accumulated on the metal surface. Additionally, the content of element C and O presented much higher values in reclaimed water than that in sterile water at 1, 5 (outer layer) and 40 days, confirming the accumulation of bacterial cells and extracellular polymeric substance (EPS). This result might be probably caused by the self-aggregation properties of microorganisms[23].

Moreover, the Cr, Ni and O elemental content in the inner layer of the 317L surface was 40.14%, 34.32% and 13.65% respectively at 5 days, probably suggesting the formation of chromium oxides or nickel oxides close to the metal base [24]. For corrosion morphology at 40 days, some corrosion products were found deposited on the periphery of the elongated IOB cells, resulting in the increase in biofilm roughness. Meanwhile, it is worth mentioning that SRB cell bodies were not clearly visible in SEM images although the SRB counts were counted in Fig. 1. Thus, it was speculated that these SRB might be located in the sublayer of the biofilm. The rapidly declining sulfate ions concentration in reclaimed water after 10 days also confirmed this speculation. And, the higher content of element S in reclaimed water experiment at 40 days was also an evidence confirming the SRB metabolic activity. And, the higher proportion of element S in reclaimed water at 40 days than that they were before, probably demonstrating that the preformed corrosion products (iron oxides and chromium oxides) might be vulcanized under the action of SRB [25, 26].

The pit corrosion of the coupons after removing the corrosion products at 40 days can be seen in Supporting Information 1 (S1). In bulk control conditions, fewer corrosion pits can be seen on the relatively smooth coupon surface. Generally, the largest pit depth was 72.2 μm. However, the pit diameter and depth of 317L SS were larger and deeper of coupons in reclaimed water. The largest corrosion depth was approximately 200.3 μm. Accordingly, this varied pit diameters and depths might be due to the difference in bacterial growth and corrosion scales morphology.

Different from the relative compact corrosion products, the corrosion scales appeared to be more porous and heterogeneous in reclaimed water experiments. This kind of coarse, inhomogeneous biofilm surface was reported promoting the initiation of localized corrosion [9], through generation of the gradients of sulfate ions and DO concentration, formation of local electrochemical cells [26, 27]. Furthermore, the sulfate ions can pass through this heterogeneous surface and can be used as electron acceptor through the SRB activity (Eq.1; Eq.2; Eq.3). This process might also enhanced the Fe depletion and facilitate the localized corrosion further [28]. Similar results have been reported on SS with SRB involved in the pit corrosion initiation [29].

$Fe \rightarrow Fe^{2+}+2e$ (anodic dissolution) (Eq.1)

$SO_4^{2-}+8H_{ad} \rightarrow S^{2-}+4H_2O$ (cathodic depolarization by SRB) (Eq.2)

$4Fe+ SO_4^{2-}+4H_2O \rightarrow 3Fe(OH)_2+FeS+2OH^-$ (overall reaction) (Eq.3)

3.3 Polarization curve analysis

Fig. 3 shows the time-dependent polarization curves of the 317L SS in sterile and reclaimed water. The curves were recorded from 1 days. The anodic branches are involved with the electron loss process from the metal base, and the cathodic branches are related to biofilm formation and metal

oxidation reaction. Compared with the control experiments, the corrosion potential (E_{corr}) of 317L in reclaimed water shift towards a more positive potential within 5 days of exposure and then shift negatively afterwards. Since the oxygen was using as the only depolarization agent, the decrease of DO concentration caused by the IOB multiplication induce the ennoblement of E_{corr} during the first 5 days. Subsequently, the rapid decrease of E_{corr} values might be attributed to the decrease of pH values that was caused by the hydrogen sulfide generation through SRB metabolic activity [22]. For better analysis, the fitted electrochemical corrosion parameters, namely, the E_{corr}, corrosion current density (i_{corr}), anodic Tafel slope (β_a) and cathodic Tafel slope (β_c) are listed in Table 2.

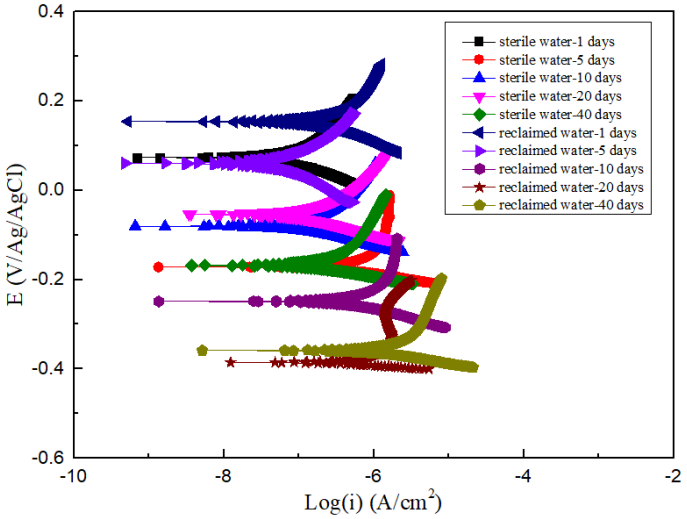

Figure 3. Polarization curves of the 317L stainless steel in sterile and reclaimed water at typical time

Table 2. Fitted results of the polarization curves in sterile water (S) and reclaimed water (R) at typical time

Tests	β_a (mV)	β_c (mV)	i_{corr} (μA/cm^2)	E_{corr} (V)
S-1 days	117	58	0.862	0.073
R-1 days	408	136	0.679	0.154
S-5 days	718	48	1.073	-0.164
R-5 days	177	154	0.154	0.060
S-10 days	197	63	0.221	-0.080
R-10 days	212	39	0.705	-0.248
S-20 days	156	76	0.236	-0.053
R-20 days	821	29	1.246	-0.385
S-40 days	250	48	0.363	-0.168
R-40 days	381	46	3.049	-0.358

The anodic current densities in sterile water decreased slightly and reached to 0.363 μA/cm^2 after 40 days exposure. The decreased i_{corr} values might be related to the accumulation of the intact oxide layer on the 317L SS surfaces. It was noteworthy that the maximum corrosion density was very small (1.073

$\mu A/cm^2$), suggesting the good corrosion resistance of 317L SS. It is speculated that this high corrosion resistance might be related to the high Cr content and the elevated Mo and Ni levels in the composition of metal base [30].

The corrosion potential of 317L SS in sterile water was -0.073 V vs. Ag/AgCl (saturated KCl) at 1 days and this value shifted to the positive side in reclaimed water. The same phenomenon can also be seen at 5 days. Additionally, i_{corr} presented lower values in reclaimed water than those in sterile water in the first 5 days. From the biofilm bacterial analysis, IOB cell counts increased sharply in the first 5 days, while SRB cell counts did not change much. Thus, it was speculated that the IOB proliferation and the EPS formation might played an inhibiting effect on the corrosion process. Moreover, the cathodic Tafel slope (β_c) values in reclaimed water were higher than those in sterile water in the first 5 days. Considering the fact that the DO served as the only cathode depolarizing agent in normal aqueous solution, there are adequate reasons to believe that the lower DO values caused by the IOB cells increased the resistance of cathodic reduction process. Although some previous studies reported that the IOB cells can enhance the corrosion of 304 SS, they presented inhibition effect of 317L SS in our study [31]. Different elemental compositions of metals might be responsible for this difference, which could change the morphology of biofilm/metal interface and alter corrosion mechanisms..

After 5 days, the polarization curves of 317L SS in reclaimed water shifted toward the negative direction significantly, making the activation region moving into high current density areas. The i_{corr} values of the working electrode in reclaimed water was nearly 3-6 times higher than that exposed to sterile water at the same duration time, suggesting a strong destructive effect of IOB and SRB biofilm on the metal surface. Moreover, the cathodic reactions were greatly polarized to the greater extent, which might be attributed to the sessile bacteria directly [32]. The much lower cathodic Tafel slope (β_c) in reclaimed water after 5 days also confirmed this conclusion. As shown in Fig. 1, the less oxygenated environment caused by the consumption of IOB metabolic activity provided a suitable environment for SRB growth in the closed, anoxic or anaerobic environment after 5 days. The accelerated cathode depolarization process caused by direct electron reduction of SRB was reported by many studies mainly including the following reasons: (1) formation of biofilm; (2) activities of hydrogenases produced by SRB; (3) consumption of active substances for cathodic depolarization of corrosion reaction; (4) changes of passive film in structure [33]. In this process, SRB could use sulphate as a terminal electron acceptor, resulting in the production of active hydrogen sulfide (H_2S) and forming the relative heterogeneous film structure. The appearance of H_2S and the local acidic environment might catalyze the anodic dissolution and induced a loss of passivity unanimously, which has been studied on nickel and iron-nickel-chromium alloys previously[29]. Fig. 3 also showed that the anodic polarization curves presented an over-passivated region at 40 days, further confirming the sulfidation effect of passive film. Consequently, despite the superior chemical corrosion resistance of 317L SS in sterile water, it could still be corroded by a biofilm with coexistence of IOB and SRB.

3.4 EIS tests

EIS was collected under a stable open circuit potential. Nyquist and Bode plots of 317L SS exposed to sterile water and reclaimed water for predetermined times are presented in Fig. 4. It showed

that the Warburg diffusion resistance presented the highest values in sterile water at 1 days, suggesting the formation of passive layer initially (Fig.4a). In Fig. 4b, three time constants can be found for the Bode plots. The peak located in the higher frequency region (>10^2 Hz) was most likely related to the outer corrosion film, while the peaks at the medium (10^0-10^2 Hz) and lower frequencies (10^{-2}-10^0) might be attributed to the inner passivation film and electron transfer resistance respectively. It has been reported that SS is prone to the formation of thin, compact protective films that shift the electron transfer resistance from the metal/water interface to the oxide/water interface. The decreased phase angles values in low frequency region showed the corrosion was also occurred in in sterile water. And, the increased phase angles values in the high frequency region (increased from 5° to 42° from 1 days to 40 days) revealed the accumulation of corrosion products on the metal surface.

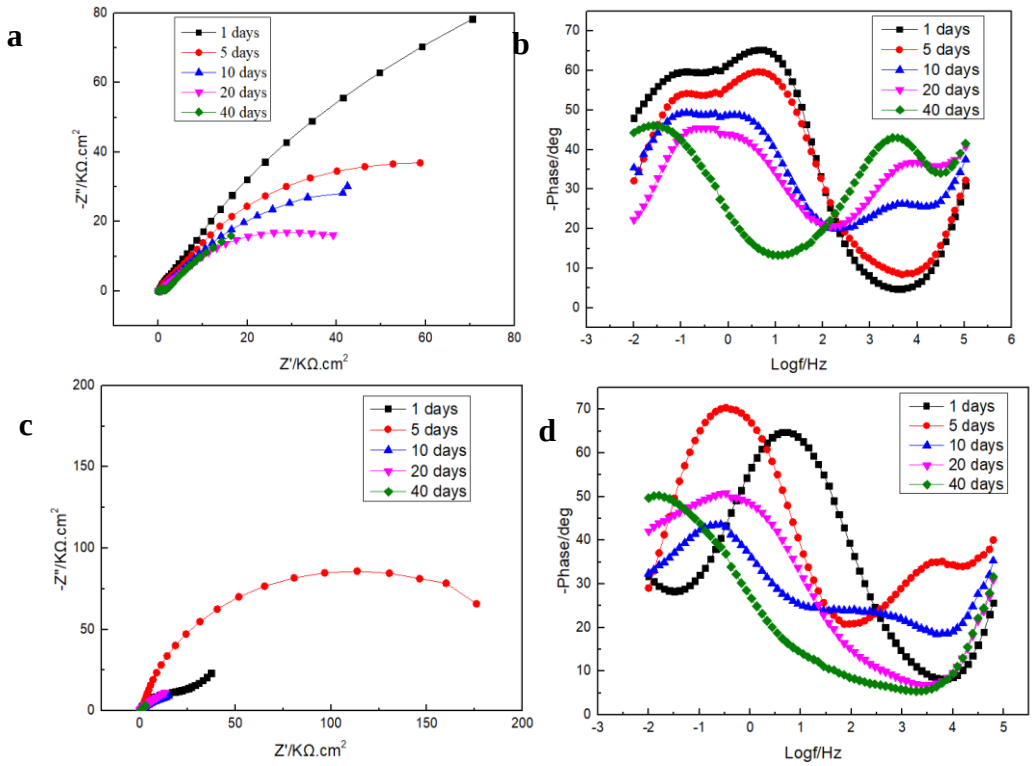

Figure 4. Nyquist and Bode plots of 317L SS in sterile water (a, b) and reclaimed water (c, d) at typical time

As shown in Fig. 4c, depressed capacitive semicircles appeared in the Nyquist plots of 317L SS in reclaimed water, which might be probably caused by bacterial adhesion or biofilm formation. Additionally, three time constants appeared in the Bode plots in the corrosion process from 1 days to 10 days (Fig. 4d), thereinto, the one in low frequency region represented the electron transfer resiatance; and the other two in intermediate frequency region and high frequency region represented the corrosion film resistance and biofilm resiatance respectively. However, there were only two time constants in the corrosion process at 20 and 40 days. The vanished peaks of Bode phase angles in intermediate frequency region probably revealed the destruction of the passivated film. The diameter of Nyquist plots in low frequency region reached the maximum values at 5 days, confirming the increase of the electron transfer

resistance. Subsequently, they decreased gradually as the bacterial growth. This result was similar to Hongwei Liu's research [13].

Moreover, the changes in the Nyquist plots with time also determined the selection of the equivalent circuit models (ECMs). The impedance spectrum of 317L SS in sterile water at 1 days showed a straight line with an angle of 45 ° in low frequency region, indicating the existence of Warburg diffusion resistance (W_o) (Fig. 4a). Thus $R_s((R_{ct}Q_{dl})(R_fQ_f)W_o)$ as shown in Fig. 5a, was used to interpretate this corrosion process. In addition, the other impedance spectras of 317L in sterile water (5, 10, 20 and 40 days) all showed three capactive semicircles. Thus, the three-time-constant model $R_s(R_{ct}Q_{dl})(Q_{fout}[R_{fout}(R_{fin}Q_{fin})])$ was used to simulate these testing results (Fig. 5b). Additionally, considering the phase angle variation, the three-time-constant model $R_s(R_{ct}Q_{dl})(Q_f[R_f(R_bQ_b)])$, was also used to simulate the corrosion process in reclaimed water experiments at 1, 5 and 10 days (Fig. 5c). Comparatively, the two-time-constant model $R_s(Q_f[R_f(R_{ct}Q_{dl})])$, as shown in Fig. 5d, was used to explain the corrosion process involving the passive film breakdown in reclaimed water at 20 days and 40 days, which was used for the interpretation of EIS data recorded in th case of 304 SS corrosion at the presence of SRB [34]. All the fitted results can be seen in Table 3, where R_s represents the electrolyte resistance; R_f and Q_f represent the resistance and constant phase element (CPE) of the corrosion film, respectively; R_b and Q_b represent the resisitance and CPE of the biofilm, respectively; R_{ct} and Q_{dl} represent the charge transfer resistance and CPE of the electrical double layer, respectively; and W represents the Warburg impedance. CPE was used to account for the dispersion effect caused by the roughness of the corrosion film or biofilm. The factor n can be used as a measure of the surface inhomogeneity and the decreased values of this factor are associated with increasing surface roughness [35]. The chi-squared (χ^2) values were all < 10^{-3}, demonstrating the high quality of the fitting results.

Table 3. Fitting parameters of 317L SS in sterile water and reclaimed water over time

3a. Fitting parameters of 317L SS in sterile water at 1 day

Times	R_s/Ω·cm^2	R_f/Ω·cm^2	Q_f/μF·cm^{-2}	n_f	R_{ct}/kΩ·cm^2	Q_{dl}/μF·cm^{-2}	n_{dl}	Wo-R /kΩ·cm^2	Wo-T /μF·cm$^{-}_{2}$	Wo-P
1 days	10.81	158.7	0.543	0.849	26.920	39.13	0.816	149.77	34.75	0.590

3b. Fitting parameters of 317L SS in sterile water at 5 days, 10 days, 20 days and 40 days

Times	R_s/Ω·cm^2	R_{fout}/Ω·cm^2	Q_{fout}/μF·cm$^{-}_{2}$	n_{fout}	R_{fin}/kΩ·cm^2	Q_{fin}/μF·cm$^{-}_{2}$	n_{fin}	R_{ct}/kΩ·cm^2	Q_{dl}/μF·cm$^{-}_{2}$	n_{dl}
5 days	23.47	222.6	0.328	0.676	27.33	46.0	0.750	121.7	63.0	0.714
10 days	28.85	914.7	0.362	0.388	38.85	65.02	0.660	115.1	77.0	0.644
20 days	25.25	161.5	1.104	0.534	144.78	78.60	0.319	81.64	62.28	0.621
40 days	15.83	1570	4.475	0.358	127.83	31.91	0.225	144.46	23.78	0.615

3c. Fitting parameters of 317L SS in reclaimed water at 1 day, 5 days and 10 days

Times	R_s/Ω·cm^2	R_f/Ω·cm^2	Q_f/μF·cm^{-2}	n_f	R_b/kΩ·cm^2	Q_b/μF·cm^{-2}	n_b	R_{ct}/kΩ·cm^2	Q_{dl}/μF·cm$^{-}_{2}$	n_{dl}

1 days	30.21	5809	28.42	0.795	28.5	0.19	0.69	154	32.37	0.605
5 days	45.15	4065	36.20	0.2455	27.9	9.36	0.55	213	20.86	0.562
10 days	15.85	3331	22.91	0.333	43.9	55.12	0.81	60.63	17.39	0.553

3d. Fitting parameters of 317L SS in reclaimed water at 20 days and 40 days

Times	$R_s/\Omega\cdot cm^2$	$R_{f+b}/\Omega\cdot cm^2$	$Q_{f+b}/\mu F\cdot cm^{-2}$	n_{f+b}	$R_{ct}/k\Omega\cdot cm^2$	$Q_{dl}/\mu F\cdot cm^{-2}$	n_{dl}
20 days	19.18	1345.2	0.368	0.400	77.92	2.577	0.618
40 days	18.76	1009.4	0.092	0.361	69.38	1.289	0.598

W_o exhibited the greatest values in sterile water at 1 days, indicating the passivation phenomenon of 317L SS. The values of W_o was 149.77 $k\Omega\cdot cm^2$ in sterile water at 1 days, which was much greater than the values of R_f, R_{ct} and R_s, demonstrating that the diffusion effect was the control steps of the corrosion process. Subsequently, the corrosion films became two different layers, including iron oxides in the outer layers (R_{fout}) and chromium and nickel oxides in the inner layers (R_{fin}) after 5 days. Moreover, the values of R_{ct}, R_{fin} all presented a decreasing tendency, showing the reduction of corrosion resistance. Additionally, the values of R_{ct} and R_{fin} were much higher than that of R_{fout} or R_s, illustrating that the electron transfer resistance and the inner chromium and nickel oxides layer was mainly responsible for the corrosion process.

In the case of 317L SS in reclaimed water, R_{ct} attained the values of 154 $k\Omega\cdot cm^2$ and 213 $k\Omega\cdot cm^2$ at 1 days and 5 days, which were higher than those in the sterile water. This indicated that the presence of IOB and SRB biofilm inhibited the electron transfer process from the metal surface in the first 5 days. Moreover, the relative higher R_f values in reclaimed water at 5 days revealed that the deposition of oxide film of iron/chromium and biofilm substantially increase the protective characteristics of 317L SS and inhibit the corrosion process.

However R_{ct} values of 317L SS in reclaimed water decreased strongly after 5 days when SRB located at a rapid growth stage (until 40 days) and the values constantly became lower than that in the sterile water. This phenomenon confirm that the SRB activity accelerated the corrosion process of 317L SS. To be specific, SRB can reduced the sulfate ions to hydrogen sulfide through its metabolic activity. And the hydrogen sulfide or sulfide could incorporate with the early-formed passivated films, catalyze its dissolution process and induce the blending of the non-protective iron sulfide or chromium sulfide layers into one, further promoting the corrosion process substantially [36]. The bode diagrams (Fig. 4d) also confirmed that only one film was found in reclaimed water in the high-frequency zone (20 days and 40 days), confirming the transformation of pre-formed corrosion layer under the effect of vulcanization.

Although many previous investigators have presumed that sulfide products can inhibit the formation of a protective oxide film, the current study focused on the invasive effect of SRB on two-layer film formation, e.g., the iron oxide layer and the chromium layer. Moreover, EDS results also revealed a greater S content in the corrosion film in reclaimed water at 40 days, confirming the sulfidation effect of SRB on the iron and chromium corrosion products further. Similar research has reported the degradation effect of SRB on the formation of chromium passivation films [37]. The relative lower n_f and n_{b+f} values in reclaimed water further confirmed the heterogeneous mixture on the metal

surface. This heterogeneous film formed on the surface due to the accumulation of bacterial metabolite and corrosion products (Fig. 2d) could induce the pit formation and propagation.

4. CONCLUSION

The corrosion process of 317L SS varied with the bacterial evolution trend of IOB and SRB cells. The decrease of DO concentration caused by the IOB multiplication induce the ennoblement of E_{corr} and the increase of cathodic Tafel slope in the first 5 days. Moreover, the deposition of an outer IOB biofilm and iron hydroxide layer and an inner chromium oxide layer increased the electron transfer resistance and retarded the corrosion process. However, after that, the SRB proliferation caused the rapid decrease of E_{corr} values and the cathodic Tafel slope through its metabolic activity and formed hydrogen sulfide after that. The hydrogen sulfide or sulfide could incorporate with the early-formed passivated films, catalyze its dissolution and induce the blending of the non-protective iron sulfide or chromium sulfide layers into one through sulphidation effect and promoting the corrosion process substantially. Moreover, the bacterial activity may cause uneven distribution of the metabolisms, generation of the gradients of sulfate ions and DO concentration and induced the larger localized corrosion in reclaimed water.

FUNDING
This work was supported by the National Natural Science Foundation of China (No. 51478307) and the Specialized Research Fund for the Doctoral Program of Higher Education of China (No. 20130032110032).

SUPPORTING INFORMATION

Pit corrosion of the 317L stainless steel in (a) sterile water and (b) reclaimed water (40 days testing)

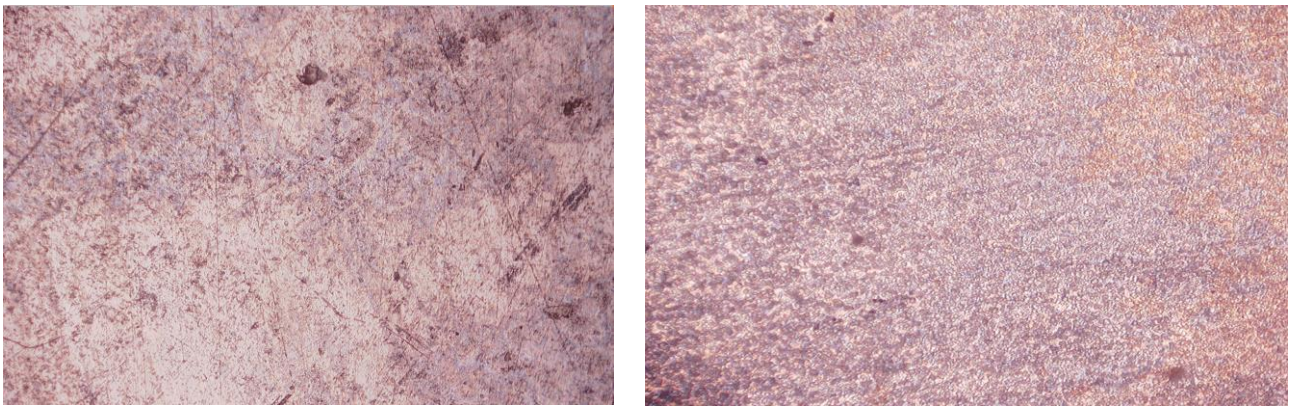

A **B**

References

1. S. J. Yuan, S. O. Pehkonen, *Corros Sci.,* 51 (2009) 1372.

2. E. Hamzah, M. F. Hussain, Z. Ibrahim, A. Abdolahi, *Arab J Sci Eng.,* 39 (2014) 6863.
3. N. O. San, H. Nazır, G. Dönmez, *Corros Sci.,* 79 (2014) 177.
4. N. B. Hallam, J. R. West, C. F. Forster, J. Simms, *Water Res.,* 35 (2001) 4063.
5. H. Liu, C. Fu, T. Gu, G. Zhang, Y. Lv, H. Wang, H. Liu, *Corros Sci.,* 100 (2015) 484.
6. N. D. Güngör, A. Çotuk, D. Dışpınar, *J Mater Eng Perform.,* 24 (2015) 1357.
7. F. Guan, X. Zhai, J. Duan, J. Zhang, K. Li, B. Hou, *Surf Coat Tech.,* 316 (2017) 171.
8. E. Ilhan-Sungur, T. Unsal-Istek, N. Cansever, *Mater Chem Phys.,* 162 (2015) 839.
9. I. B. Beech, J. A. Sunner, K. Hiraoka, *Int Microbiol.,* 8 (2005) 157.
10. H. Castaneda, X. D. Benetton, *Corros Sci.,* 50 (2008) 1169.
11. K. Alasvand Zarasvand, V.R. Rai, *Int Biodeter Biodegr.,* 87 (2014) 66.
12. D. Starosvetsky, R. Armon, J. Yahalom, J. Starosvetsky, *Int Biodeter Biodegr.,* 47 (2001) 79.
13. Y. H. Zhang, C. M. Xu, G. X. Cheng, *Inorg Mater.,* 43 (2007) 614.
14. H.Z. Wadood, A. Rajasekar, Y. Ting, A.N. Sabari, *Arab J Sci Eng.,* 40 (2015) 1825.
15. F. Batmanghelich, L. Li, Y. Seo, *Corros Sci.,* 121 (2017) 94.
16. J. Wu, D. Zhang, P. Wang, Y. Cheng, S. Sun, Y. Sun, S. Chen, *Corros Sci.,* 112 (2016) 552.
17. S. K. Karn, G. Fang, J. Duan, *Front Microbiol.,* 8 (2017) 2038
18. D. Xu, J. Xia, E. Zhou, D. Zhang, H. Li, *Bioelectrochemistry.,* 113 (2017) 1.
19. Z. H. Sun, M. Moradi, Y. X. Chen, R. Bagheri, P. S. Guo, L. J. Yang, Z. L. Song, C. Xu, *Mater. Chem. Phys., 208, 149-156.*, (2018) 149.
20. M. Moradi, J. Duan, H. Ashassi-Sorkhabi, X. Luan, *Corros Sci.,* 12 (2011) 4282.
21. J. Michalska, B. Chmiela, W. Simka,. *Mater Corros*., 69 (2018) 1047
22. Y. Wan, D. Zhang, H. Q. Liu, Y. j. Li, B. Hou, *Electrochim Acta.,* 55 (2010) 1528.
23. P. J. Antony, R K Singh Raman, R. Raman, P. Kumar, *Corrosion. Sci.,* 52 (2010) 1404.
24. Y. Cui, S. Liu, K. Smith, H. Hu, F. Tang, Y. Li, K. Yu, *J Environ Sci-China.,* 48 (2016) 79.
25. W. Dec, M. Mosiałek, R. P. Socha, M. Jaworska-Kik, W. Simka, J. Michalska, *Mater. Chem. Phys.,* 195 (2017).
26. A. A. Steele, D. T. Goddard, I. B. Beech, *Int. Biodeter. Biodegr.,* 34 (1994) 35.
27. J. Duan, B. R. Hou, Z. G. Yu, *Mat. Sci. Eng. C.,* 26 (2006) 624.
28. D. Enning, J. Garrelfs, *Appl Environ Microb.,* 80 (2014) 1226.
29. F. Li, M. An, G. Liu, D. Duan, *Mater. Chem. Phys.,* 113 (2009) 971.
30. Chen G, Clayton C. R., *J. Electrochem. Soc.,* 145 (1998) 1914.
31. J. Starosvetsky, D. Starosvetsky, B. Pokroy, T. Hilel, R. Armon, *Corros Sci.,* 50 (2008) 540.
32. W. H. Dickinson, Z. Lewandowski, *Biodegradation.,* 9 (1998) 11.
33. H. Venzlaff, D. Enning, J. Srinivasan, K. J. J. Mayrhofer, A. W. Hassel, F. Widdel, M. Stratmann, *Corros Sci.,* 66 (2013) 88.
34. J. E. G. González, A. F. J. H. Santata, J. C. Mirza-Rosca, *Corros Sci.,* 40 (1998) 2141.
35. H H P Fang, K Y Chan , L. C. Xu, *J. Microbiol. Methods.,* 40 (2000) 89.
36. P.J. Antony, S. Chongdar, P. Kumar, R. Raman, *Electrochim Acta.,* 52 (2007) 3985.